ADVANCED ENERGY MATERIALS

Supporting Information

for *Adv. Energy Mater.,* DOI: 10.1002/aenm.202202029

Interfacial Embedding for High-Efficiency and Stable Methylammonium-Free Perovskite Solar Cells with Fluoroarene Hydrazine

Dhruba B. Khadka, Yasuhiro Shirai,* Masatoshi Yanagida, Terumasa Tadano, and Kenjiro Miyano*

Supporting Information

Interfacial Embedding for High-Efficiency and Stable Methylammonium-Free Perovskite Solar Cells with Fluoroarene Hydrazine

Dhruba B. Khadka[1]*, Yasuhiro Shirai[1#], Masatoshi Yanagida[1], Terumasa Tadano[2], and Kenjiro Miyano[1]

[1] Photovoltaic Materials Group, Center for GREEN Research on Energy and Environmental Materials, National Institute for Materials Science (NIMS), 1-1 Namiki, Tsukuba, Ibaraki 305-0044, Japan

[2] Research Center for Magnetic and Spintronic Materials, National Institute for Materials Science (NIMS), 1-2-1 Sengen, Tsukuba, Ibaraki 305-0047, Japan.

Corresponding Author

*KHADKA.B.Dhruba@nims.go.jp

*SHIRAI.Yasuhiro@nims.go.jp

Table and Figures

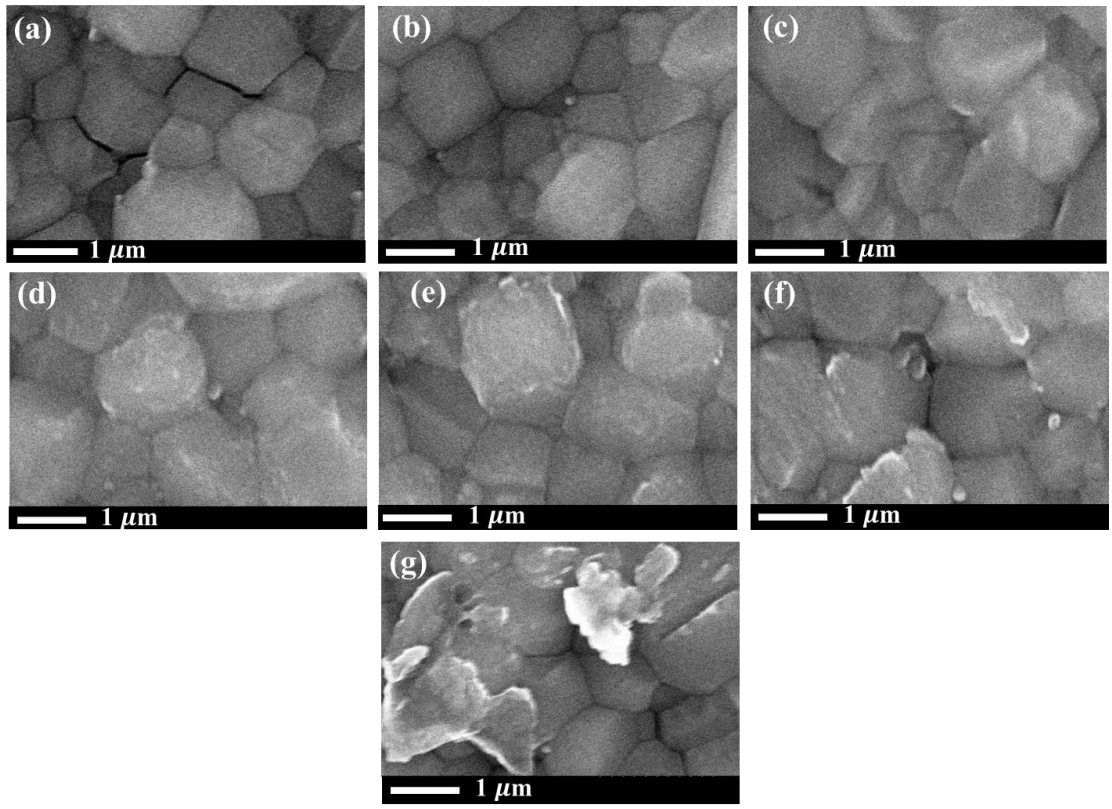

Figure S1. SEM images of MA-free ($FA_{0.84}$ $Rb_{0.04}Cs_{0.12}PbI_3$) films with 5F-PHZ treatment; 5F-PHZ solutions in IPA; (a) control, (b) 0.5 mol%, (c) 1 mol%, (d) 2 mol%, (e) 3 mol %, (f) 5 mol%, (g) 10 mol %.

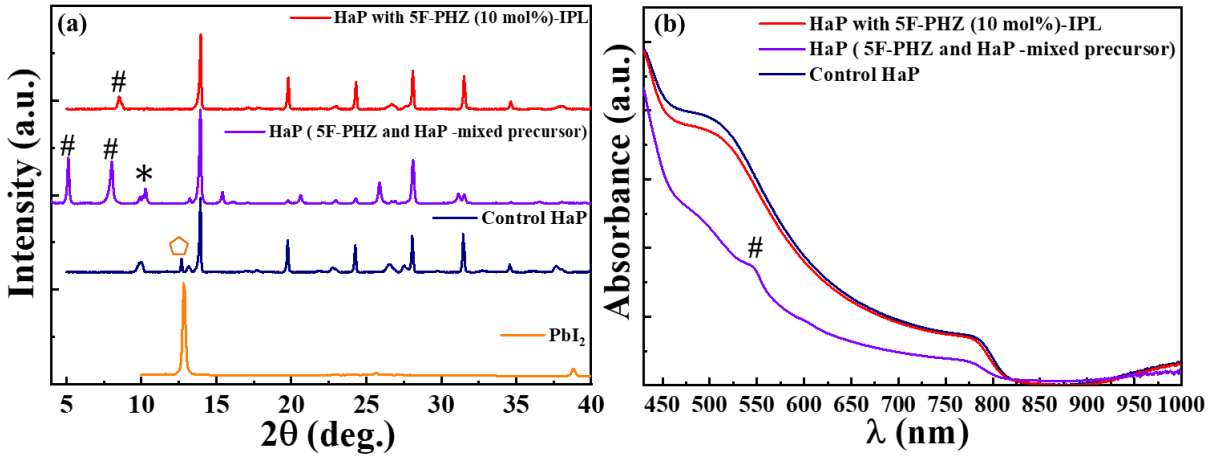

Figure S2. XRD patterns (a) of PbI_2 film, control HaP film, perovskite film prepared using 5F-PHZ/perovskite-mixed precursor, and HaP film with 5F-PHZ (dissolved10 mol% in IPA) treatment. (b) absorption spectra respective perovskite films. Here,□- PbI_2 peak, *- δ-perovskite phase, and # -2D phase with 5F-PHZ. The shoulder response marked with # in absorption spectra stem from 2D phase

formed with 5F-PHZ. Note that 5F-PHZ and HaP- mixed precursor was prepared by mixing 0.5M-5F-PHZ + 0.5 M PbI_2 and 1M of control precursor ($FA_{0.84}$ $Rb_{0.04}Cs_{0.12}PbI_3$).

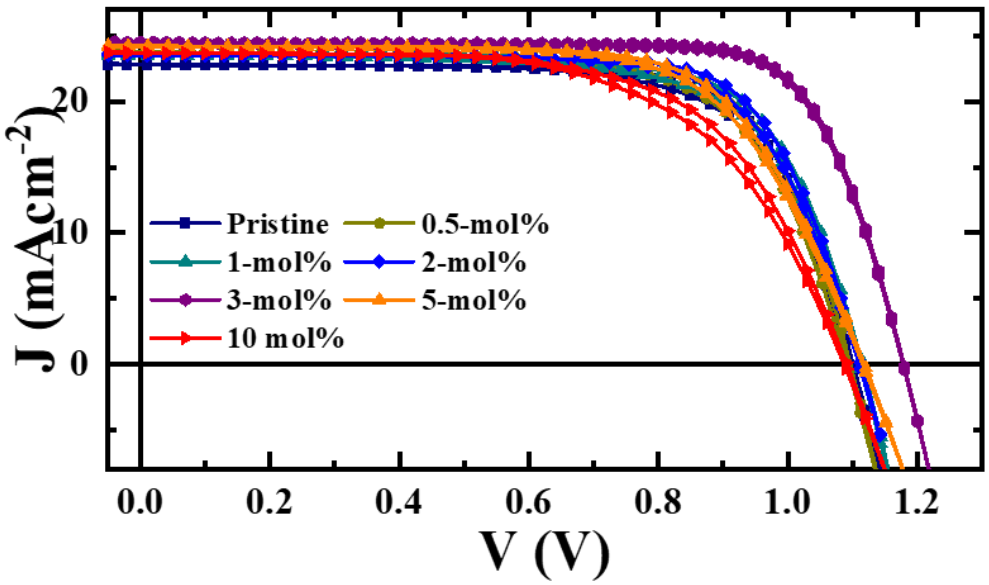

Figure S3. *J-V* characteristics of PSCs with 3D-perovskite film; $FA_{0.84}$ $Rb_{0.04}Cs_{0.12}PbI_3$, treated with 5F-PHZ-IPA solution with varying concentrations. (0-10 mol%). The double line of J-V curves for each case represents forward and reverse scan directions.

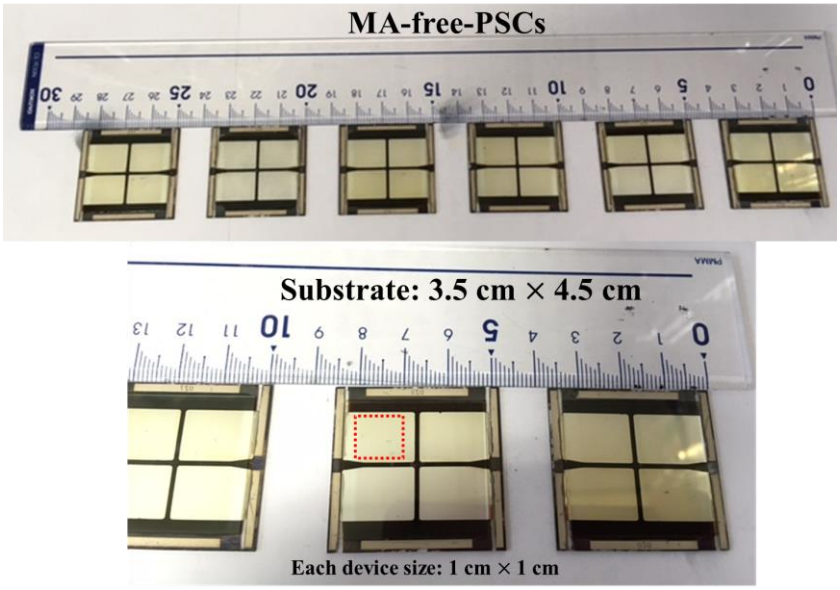

Figure S4. Photographs of a set of complete HaP devices prepared on ITO substrate (4.5 cm ×3.5 cm) and scale of each device size (1cm×1cm) used for measurement mask.

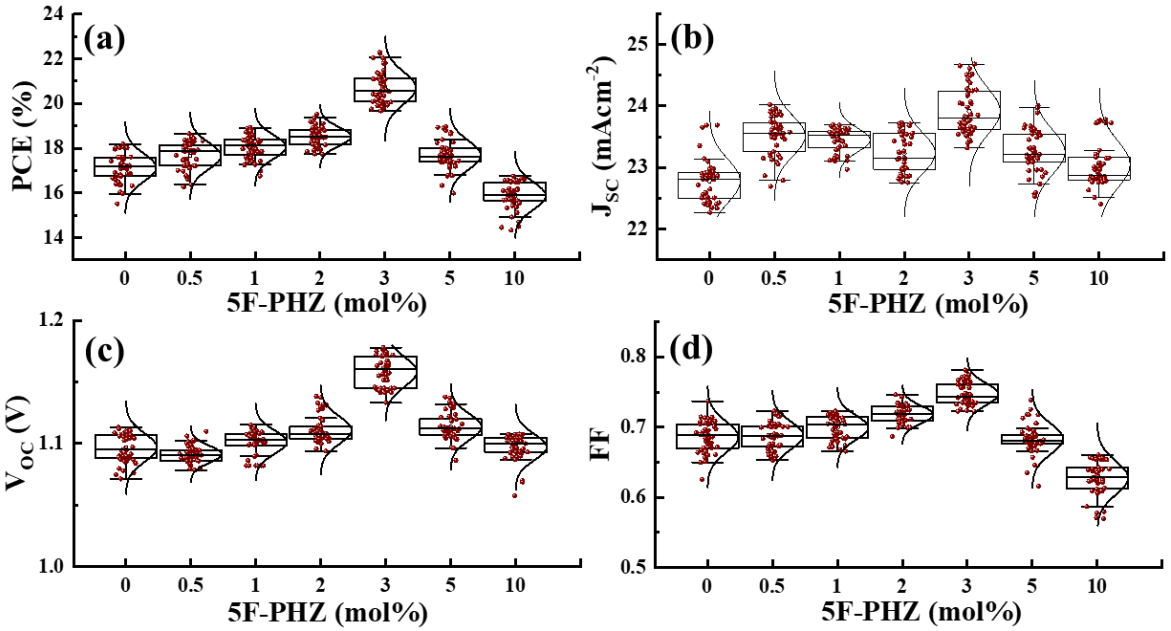

Figure S5. Statistics of photovoltaic parameters of control and with 5F-PHZ treatment PSCs, including V_{OC}, J_{SC}, FF, and PCE. These data consist of 30 devices from 5 batches for each 5F-PHZ concentration.

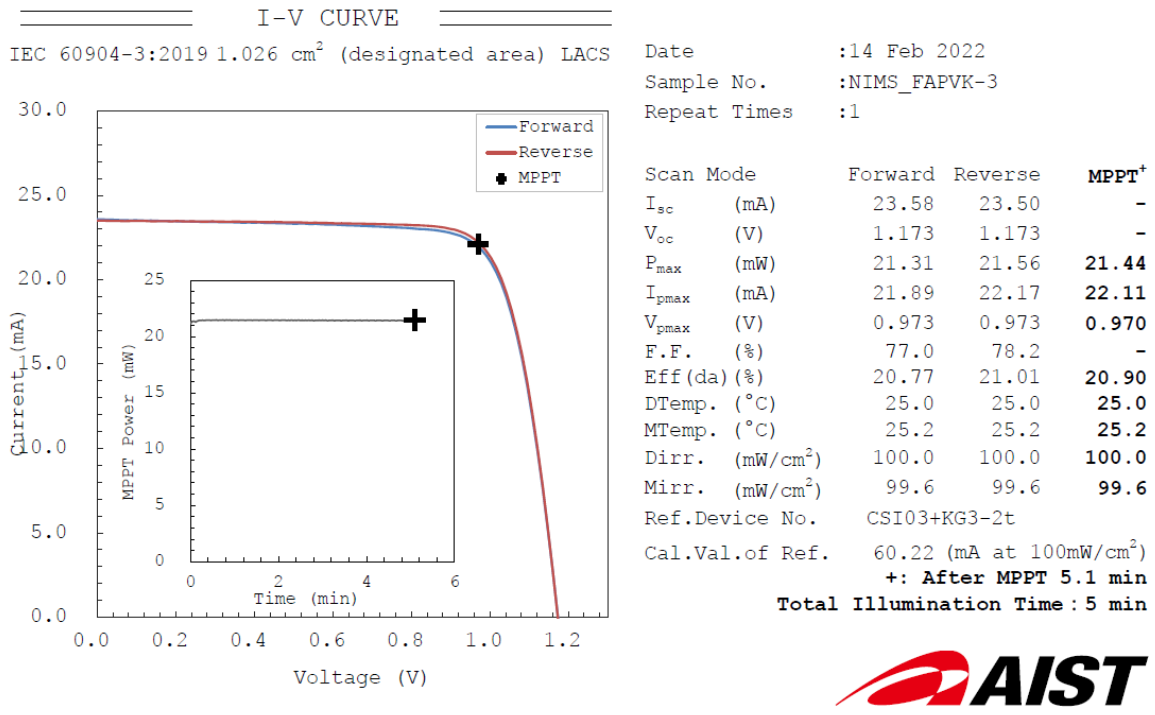

Figure S6. Certified results from an accredited photovoltaic certification laboratory (AIST, Japan). The certified J-V curves (RB-HaP film: $Rb_{0.4}Cs_{0.12}FA_{0.84}PbI_3$ with 5F-PHZ surface treatments) with

double scanning give PCE forward: 20.77% and PCE reverse: 21.01% with large device area of 1.026 cm^2.

Table S1. Summary of certified/record device large area (1 cm^2) reports (Pb-perovskite using multiple cations, anions, functional additives, and interfacial layer).

Device Type	Device Structure	Perovskite	Additive	Area (cm^2)	PCE (%)	Reported Efficiency	date	Ref.
Regular (n-i-p)	Glass/ITO/c-TiO_2/TiO_2 nanorods/PMMA:PCBM/ **Perovskite**/PMMA/Spiro-OMeTAD)/MoOx/IZO/**Au**	(Cs,FA,MA)Pb($I,Br)_3$	-----	1.0	21.6	Certified	2021	[1]
Regular (n-i-p)	Glass/FTO/TiO_xN_y/meso-TiO_2/PMMA: PCBM/ **perovskite**/PMMA/P_3HT: CuPc/**Au**	(Cs,FA,MA)Pb($I,Br)_3$	0.01 M-PbCl2, 0.01 M-MACl	1.0	22.6	Certified	2022	[2]
Regular (n-i-p)	Glass/FTO/SnO2/ **perovskite**/spiro-OMeTAD /EVA/**Cu-Ni-Graphene**	FAMAPb(I,B_r)3	-----	0.09	24.37	Certified	2022	[3]
				1.02	20.76			
Inverted (p-i-n)	Glass/ITO/NiOx-nanoparticles/ (IL)EMDP/ **Perovskite**/PCBM/BCP/**Au**	($Cs,FA,MA)Pb(I,B_r)_3$	-----	1.01	20.91	Not certified	2021	[4]
Regular (n-i-p)	Glass/FTO/SnO_2(ALD)/PCBM/PMMA/**Perovskite**/PMMA/Spiro/**Au**	(Rb,Cs,FA)PbI_3	-----	0.1024	20.35	Not certified	2018	[5]
Inverted (p-i-n)	Glass/ITO/2PACz/**Perovskite/PEACl**/C_{60}/BCP/**Au**	(Cs,FA)PbI_3	phenethylammonium chloride	0.123	22.3	Not certified	2021	[6]
Inverted (p-i-n)	Glass/ITO/NiOx-sputtered/ MeO/**Perovskite**/5F-PHZ/ C_{60}/BCP/**Ag**	(Rb,Cs,FA)PbI_3	5F-PHZ	1.026	21.01 (22.29)	Certified	*This work (Record certify PCE for inverted device structure)	

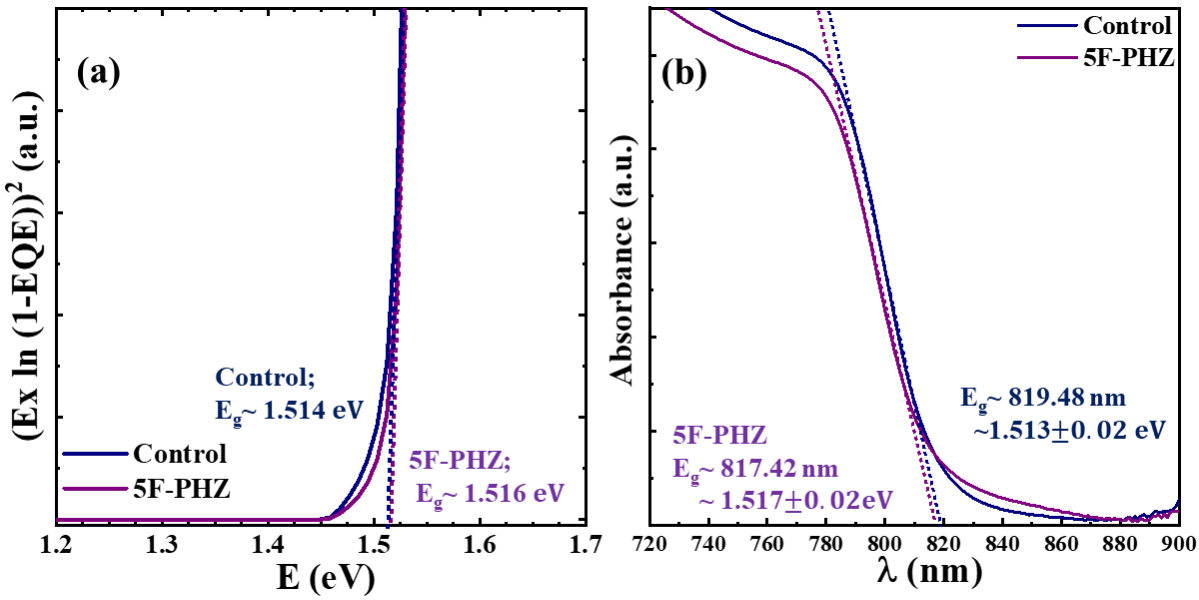

Figure S7. Estimation of bandgap energy (E_g) of HaP layer in control and 5F-PHZ PSCs. (a) E_g estimated from EQE analysis and (b) E_g calculated from absorption spectra of respective films.

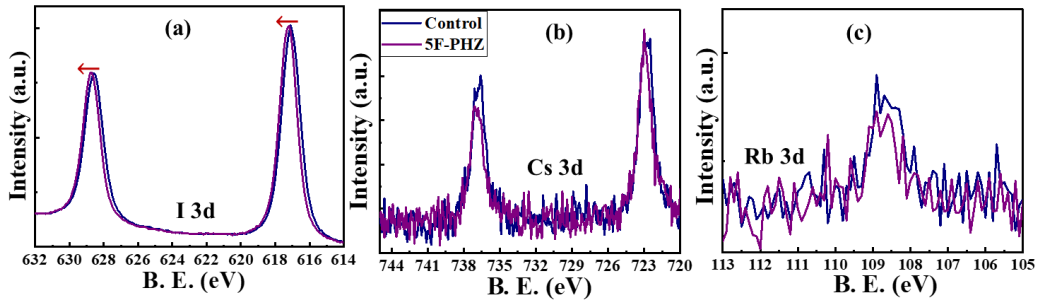

Figure S8. XPS-spectra for the control and 5F-PHZ treated films; I-3d core (a), Cs-3d core (b), and Rb-3d core (c). Arrow head indicates shifting direction of XPS characteristic peak.

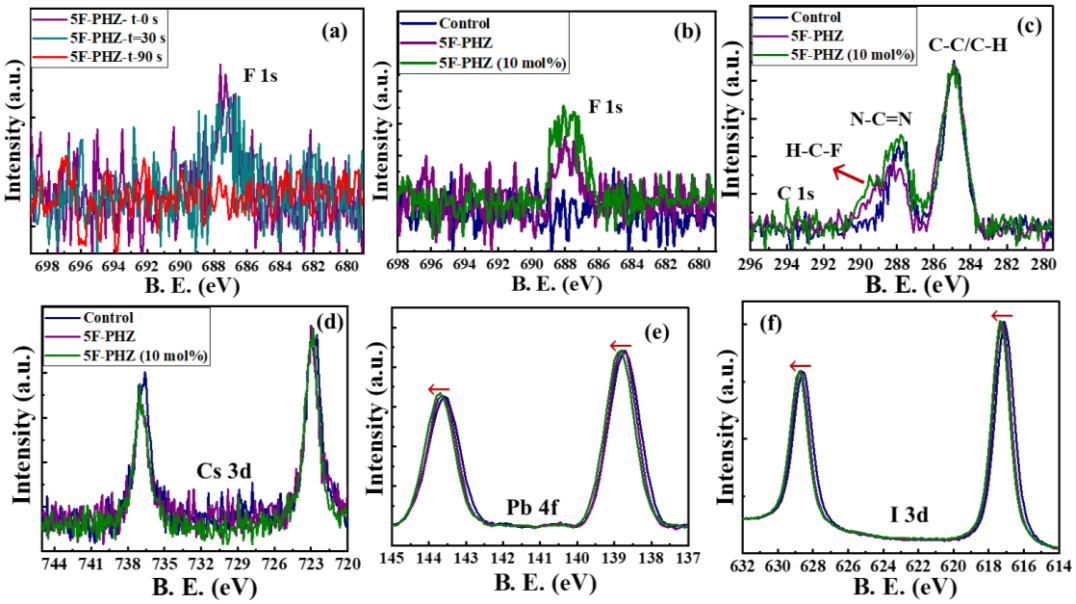

Figure S9. XPS-spectra for the control and 5F-PHZ treated films. F-1s core with Depth profile of 5F-PHZ treatment (a). A comparison of XPS spectra control, 5F-PHZ (optimal, 3 mol%) and 5F-PHZ (5 mol%); F-1s core (b), C-1s core (c), Cs-3d (d), Pb-4f core (e), and I-3d core (f). Arrowhead indicates shifting direction of XPS characteristic peak.

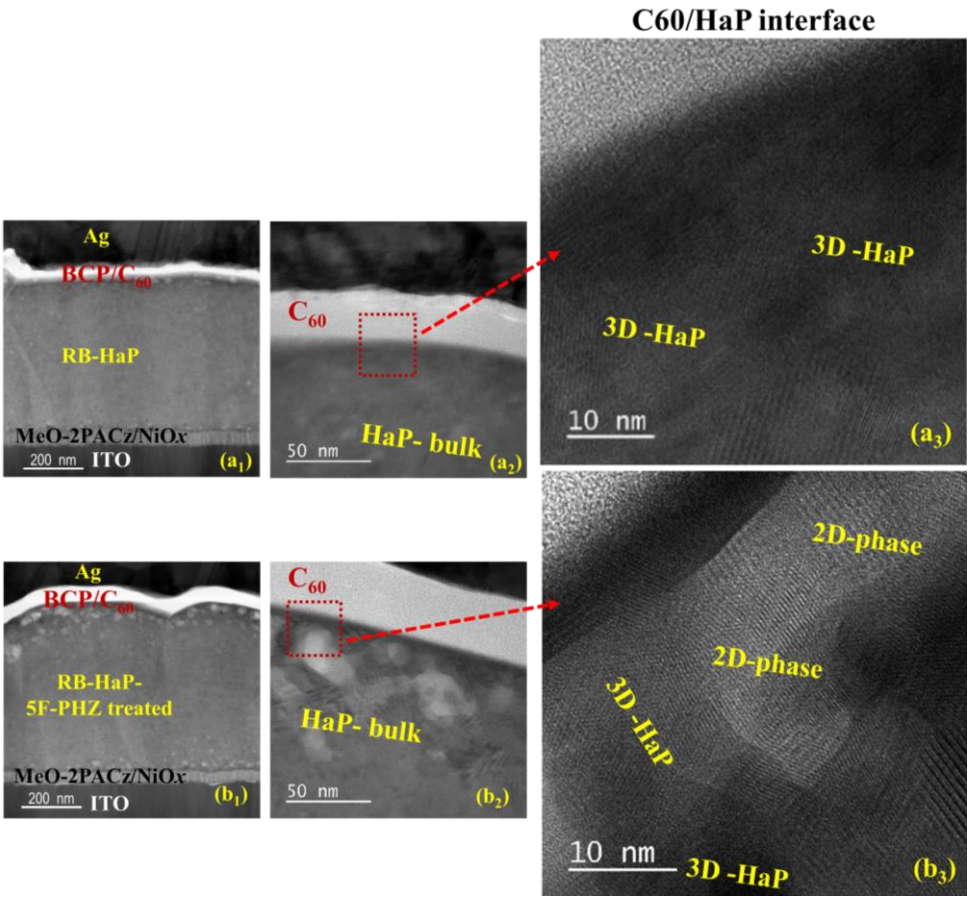

Figure S10. Cross-sectional HR-TEM image of RB-PSCs; control (a_1) and 5F-PHZ treatment (b_1). Interface of C_{60}/HaP (a_2, b_2) and the interface of C_{60}/HaP top surface (a_3, b_3). Note that 2D-phase formed with 5F-PHZ distributes unevenly on the surface of 3D-HaP or at grain boundaries.

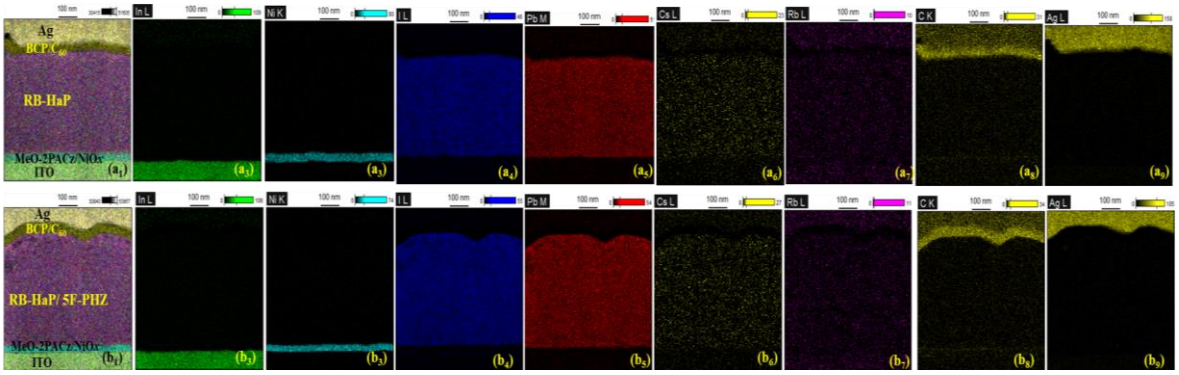

Figure S11. STEM-EDX mapping of the control (a) and 5F-PHZ treated device for RB-PSCs (b). The EDX mapping of respective layer is displayed in respective row. ITO- In (a_2, b_2), NiOx-Ni (a_3, b_3), HaP; -I (a_4, b_4), Pb (a_5, b_5), Cs (a_6, b_6), Rb (a_7, b_7), PCBM- C (a_8, b_8), Ag-electrode-Ag (a_9, b_9).

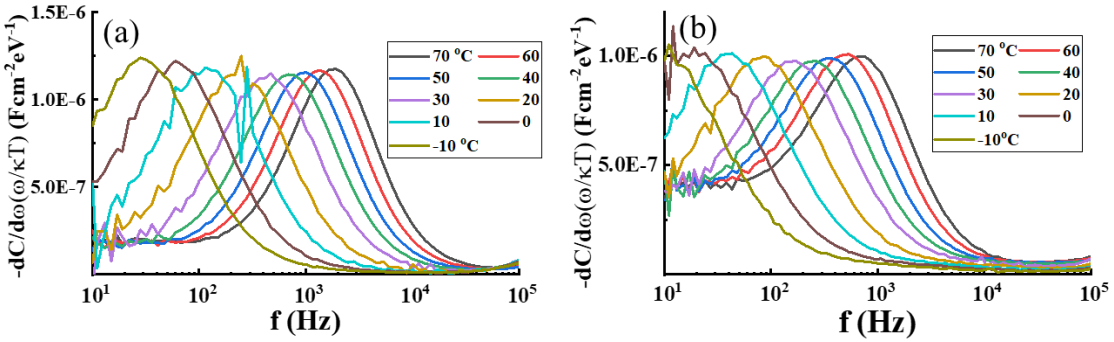

Figure S12. Differentiation of C-f spectra for determination of inflection frequencies; control device (a) and 5F-PHZ treated device (b).

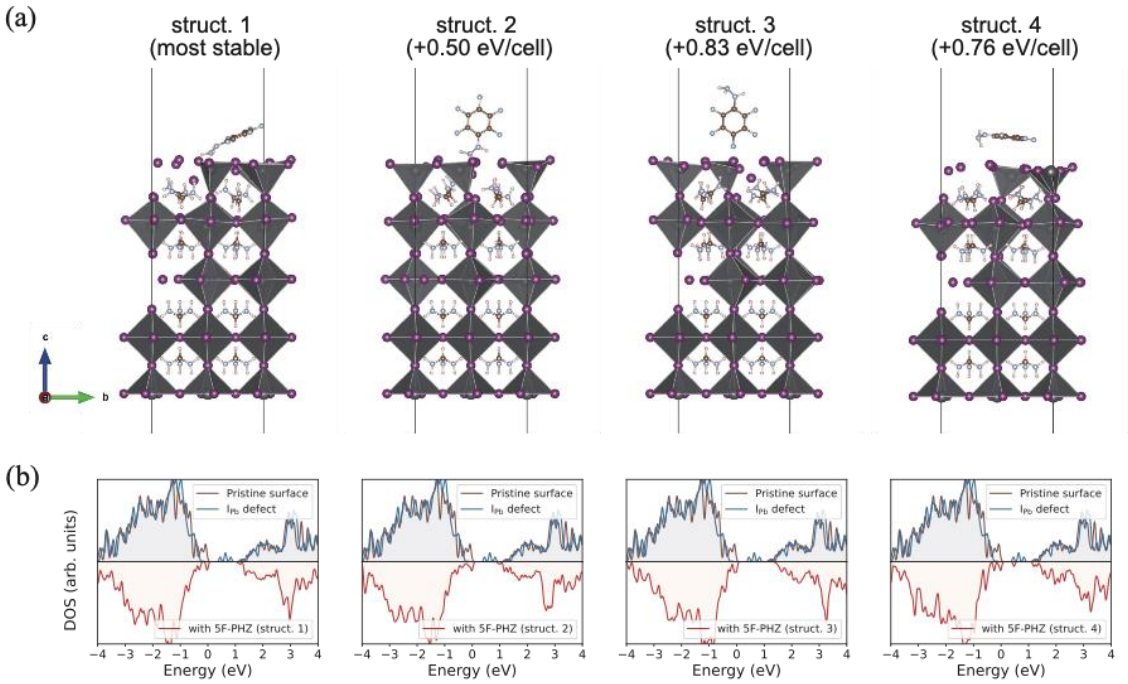

Figure S13. Atomic structures and associated density of states (DOS) of 5F-PHZ passivated surfaces obtained from DFT calculations. (a) Side views of the (meta-)stable structures of a 5F-PHZ molecule on PbI_2-terminated surface with an I_{Pb} antisite defect. The struct. 1 is the most stable structure we obtained, and other three structures are less stable by the energy values shown in the parentheses. (b) Calculated DOS of the four structures shown in (a). For the pristine and the 5F-PHZ passivated surfaces, the energy (x-axis) is measured relative to their valence band maximum. For the I_{Pb} defected surface, the x-axis value is slightly adjusted in such a way that the position of the conduction band minimum, which is calculated after neglecting the in-gap state, matches with that of the pristine surface. In the main text, we show the results for the most stable structure (struct. 1).

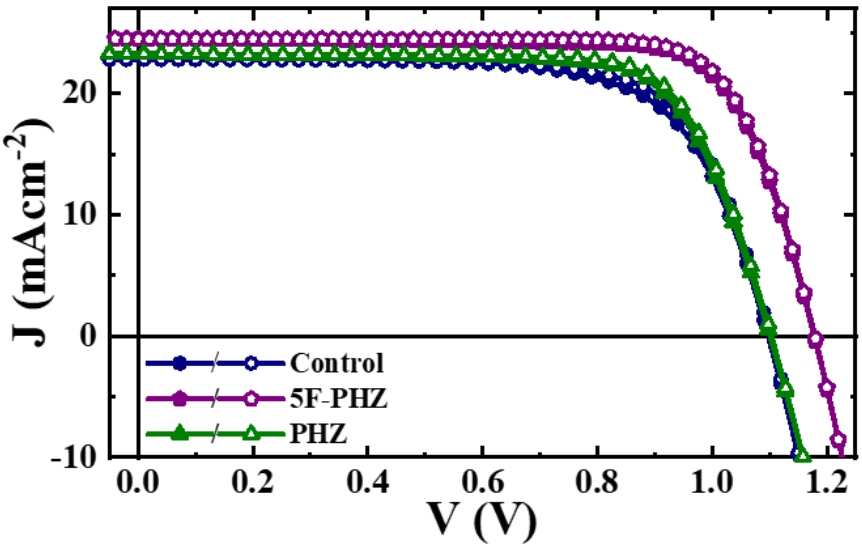

Figure S14. *J-V* curves (device parameters Table S2) (▼forward /s reverse scan direction) of control, PHA, and 5F-PHZ treated devices measured under AM 1.5G illumination for RB-HaP; $Rb_{0.04}Cs_{0.12}FA_{0.84}PbI_3$.

Table S2. Photovoltaic parameters of the best performing RB-PSCs (control, PHA, and 5F-PHZ treatment). F and R- scan stand for forward and reverse scan directions. The statistical data (control, PHA, and 5F-PHZ treatment) are taken from 16 devices (average (avg) and standard deviation (sd)) from 4 batches.

Device parameters	RB-HaP: $Rb_{0.04}Cs_{0.12}FA_{0.84}PbI_3$ - RB-PSCs								
	Control			PHA			5F-PHZ		
	Best result		Statistics (avg ±sd)	Best result		Statistics (avg ±sd)			Statistics (avg ±sd)
	F-scan	R-scan		F-scan	R-scan		F-scan	R-scan	
J_{SC} (mA/cm^2)	22.874	22.88	22.67 ±0.34	23.28	23.24	23.03 ±0.34	24.55	24.51	24.05 ±0.37
V_{OC} (V)	1.098	1.096	1.09 ±0.015	1.101	1.105	1.10 ±0.035	1.1765	1.178	1.163 ±0.011
FF	0.6952	0.722	0.692 ±0.0185	0.734	0.752	0.731 ±0.0286	0.761	0.772	0.752 ±0.0164
R_s (Ωcm^{-2})	5.41	5.23		5.7	5.52		4.96	4.90	
R_{sh} (kΩcm^{-2})	2.55	5.37		3.21	8.51		3.51	7.88	
PCE (%)	17.45	18.10	17.26 ±0.64	18.81	19.31	19.12 ±0.62	21.98	22.29	21.03 ±0.65

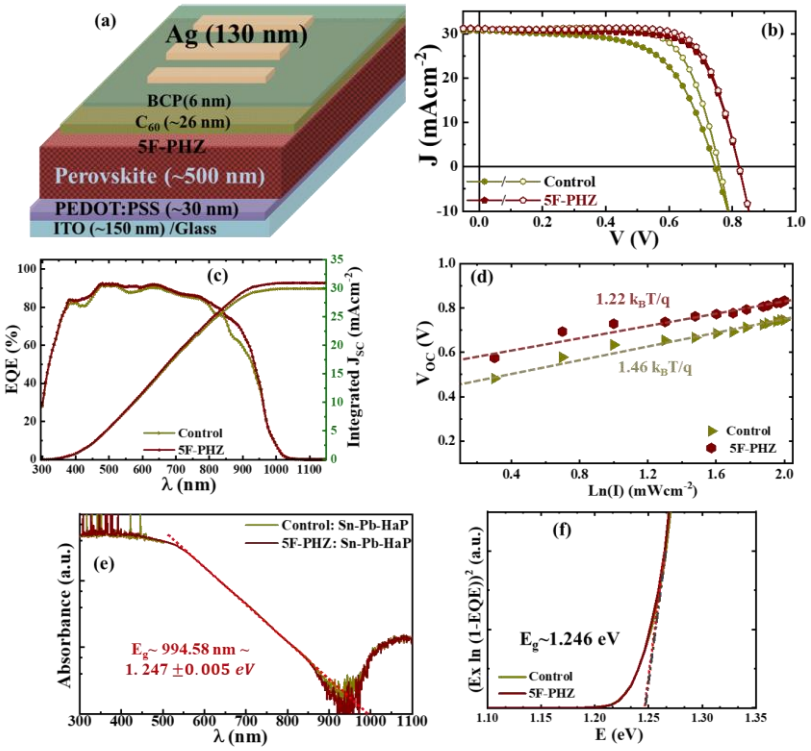

Figure S15. Schematic of device architecture (ITO/PEDOT:PSS/NB-HaP/C_{60}/BCP/Ag) (a). *J-V* curves (device parameters Table S3) (b) (▼forward /s reverse scan direction). *EQE* spectra (c) of control and 5F-PHZ treated devices measured under AM 1.5G illumination for NB-HaP; Sn-Pb-HaP; $FA_{0.85}MA_{0.1}Cs_{0.05}(Pb_{0.5}Sn_{0.5})I_3$. The values of integrated J_{SC} extracted from *EQE* spectra; 29.80 and 30.64 $mAcm^{-2}$. Diode ideality factor extracted from intensity dependent-V_{OC} (d). Estimation of bandgap energy (E_g) of NB-HaP layer in control and 5F-PHZ PSCs from the absorption spectra (e) and EQE analysis (f).

Table S3. Photovoltaic parameters of the best performing NB-PSCs (control and 5F-PHZ treatment). F and R- scan stand for forward and reverse scan directions. The statistical data (control or 5F-PHZ treatment) are taken from 16 devices (average (avg) and standard deviation (sd)) from 4 batches.

Device parameters	NB-HaP: $FA_{0.85}MA_{0.1}Cs_{0.05}(Pb_{0.5}Sn_{0.5})I_3$- *NB-PSCs*					
	Control			5F-PHZ		
	best result		statistics (avg±sd)	best result		Statistics (avg±sd)
	F-scan	R-scan		F-scan	R-scan	
J_{SC} (mA/cm^2)	30.68	30.72	30.36 ±0.52	31.08	31.16	30.86 ±0.36
V_{OC} (V)	0.743	0.758	0.741 ±0.013	0.821	0.831	0.813 ±0.011
FF	0.631	0.722	0.663 ±0.038	0.711	0.747	0.72 ±0.021
R_s (Ωcm^{-2})	3.33	2.98		2.94	2.92	
R_{sh}($k\Omega cm^{-2}$)	5.93	15.14		24.77	38.42	
PCE (%)	14.38	16.81	15.23 ±0.98	18.14	19.34	18.74 ±0.57

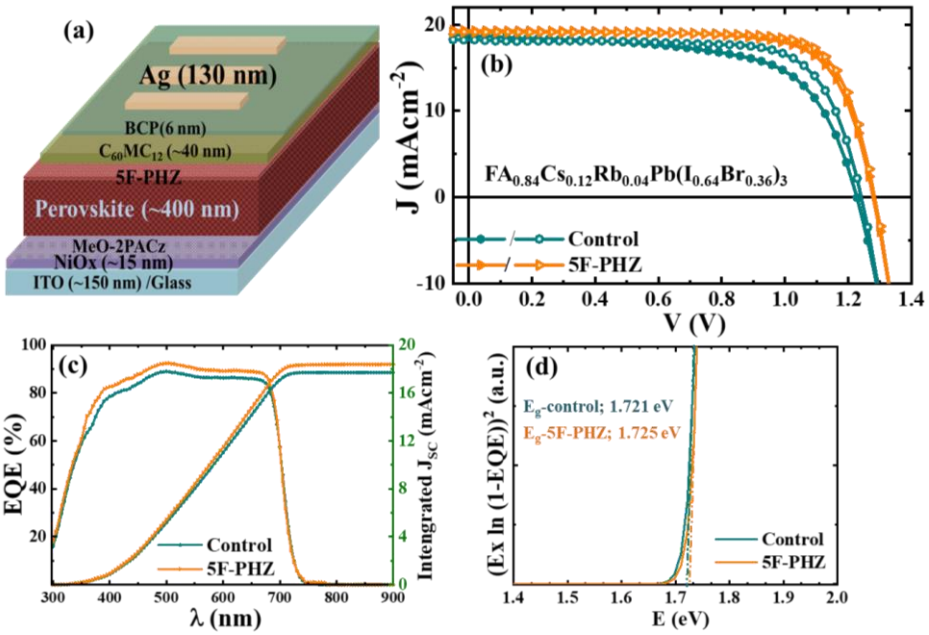

Figure S16. Schematic of device architecture (WB-PSCs) (ITO/NiO_x/MeO-2PACz/WB-HaP/$C_{60}MC_{12}$/BCP/Ag) (a). *J-V* curves (device parameters Table S4) (b) (▼forward /s reverse scan direction). *EQE* spectra (c) of control and 5F-PHZ treated devices measured under AM 1.5G illumination for MA-free wide-bandgap halide perovskite (WB-HaP); $FA_{0.84}Cs_{0.12}Rb_{0.04}Pb(I_{0.63}Br_{0.37})_3$ system. The values of integrated J_{SC} extracted from *EQE* spectra; 17.72 and 18.39 $mAcm^{-2}$. Estimation of bandgap energy (E_g) of WB-HaP layer in control and 5F-PHZ PSCs from the EQE analysis (d). For WB-PSCs, we adopted the halide composition as reported by Snaith and co-workers[7] and our previous report.[8] Similarly, the ETL layer; C_{60}-fused *N*-methylpyrrolidine-*meta*-dodecyl phenyl ($C_{60}MC_{12}$) was used as reported in our earlier report for WB-PSC.[8]

Table S4. Photovoltaic parameters of the best performing WB-PSCs (control and 5F-PHZ treatment). F and R- scan stand for forward and reverse scan directions. The statistical data (control or 5F-PHZ treatment) are taken from 16 devices (average (avg) and standard deviation (sd)) from 4 batches.

Device parameters	WB-HaP: $FA_{0.84}Cs_{0.12}Rb_{0.04}Pb(I_{0.63}Br_{0.37})_3$- *WB-PSCs*					
	Control			5F-PHZ		
	best result		statistics (avg±sd)	best result		Statistics (avg±sd)
	F-scan	R-scan		F-scan	R-scan	
J_{SC} (mA/cm^2)	18.75	18.24	17.82±0.56	19.32	19.28	19.18 ±0.114
V_{OC} (V)	1.234	1.241	1.240 ±0.0041	1.282	1.283	1.279 ±0.0034
FF	0.649	0.739	0.707 ±0.033	0.737	0.765	0.74 ±0.016
R_s (Ωcm^{-2})	5.92	5.53		4.69	4.81	
R_{sh} (kΩcm^{-2})	2.48	3.62		5.74	11.18	
PCE (%)	15.01	16.73	15.62 ±0.71	18.27	18.92	18.32 ±0.42

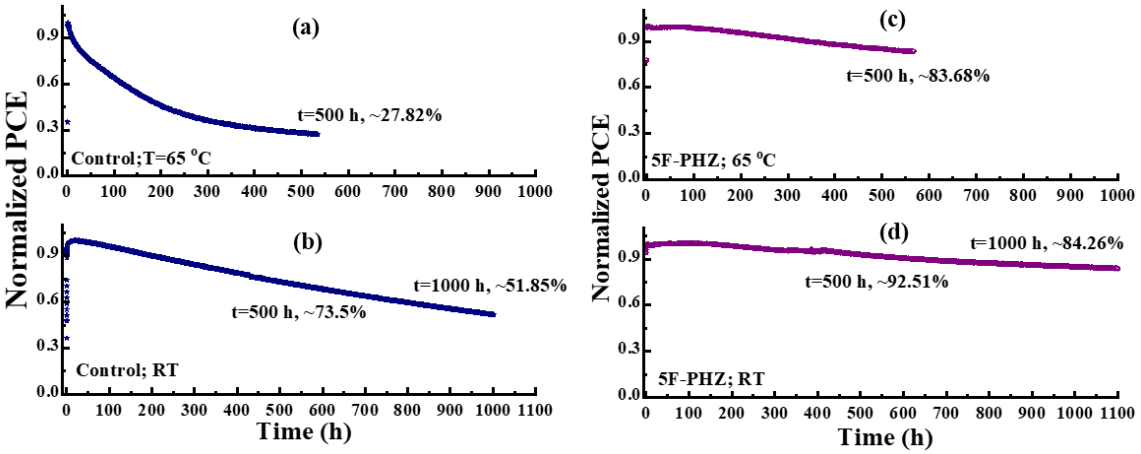

Figure S17. Operational stability of the control and 5F-PHZ treated devices (RB-HaP; E_g~1.52 eV). The devices were kept under 1-Sun intensity under MPPT conditions (35–40% RH, 27–32 °C~RT (a, c) and elevated temperature ~65 °C (b, d)) during device stability monitoring.

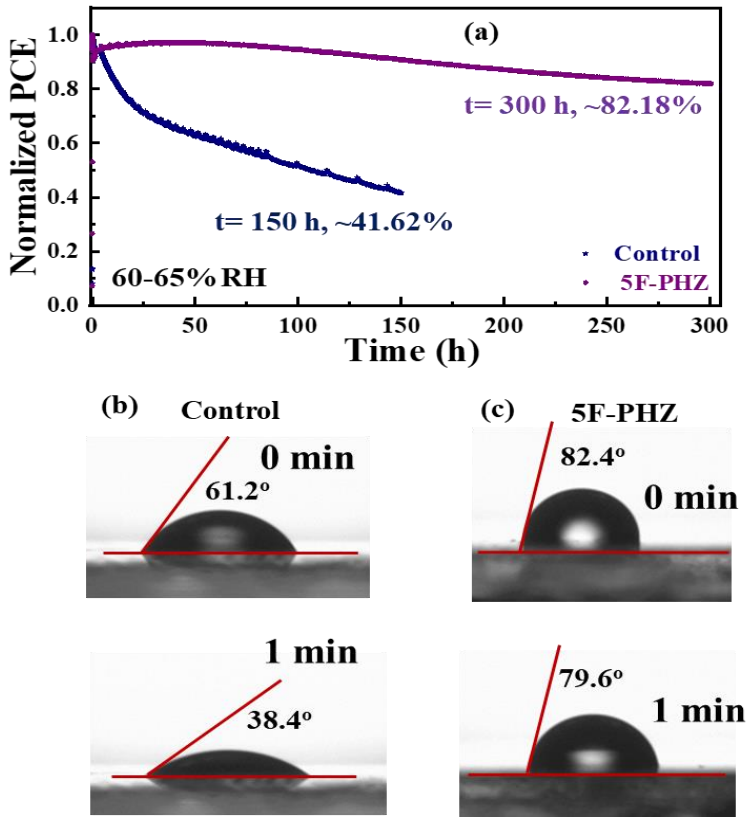

Figure S18. Operational stability of the control and 5F-PHZ treated devices (RB-HaP; E_g~1.52 eV). The devices were kept under 1-Sun intensity under MPPT conditions (60–65% RH, 27–32 °C~RT) (a). Images of the water contact angle on the surface of (b) control and (c) 5F-PHZ treated perovskite films at different water loading times (initial (0 min) and after 1 min).

References

[1] J. Peng, D. Walter, Y. Ren, M. Tebyetekerwa, Y. Wu, T. Duong, Q. Lin, J. Li, T. Lu, M. A. Mahmud, O. L. C. Lem, S. Zhao, W. Liu, Y. Liu, H. Shen, L. Li, F. Kremer, H. T. Nguyen, D.-Y. Choi, K. J. Weber, K. R. Catchpole, T. P. White, *Science* **2021**, *371*, 390.

[2] J. Peng, F. Kremer, D. Walter, Y. Wu, Y. Ji, J. Xiang, W. Liu, T. Duong, H. Shen, T. Lu, F. Brink, D. Zhong, L. Li, O. Lee Cheong Lem, Y. Liu, K. J. Weber, T. P. White, K. R. Catchpole, *Nature* **2022**, *601*, 573.

[3] X. Lin, H. Su, S. He, Y. Song, Y. Wang, Z. Qin, Y. Wu, X. Yang, Q. Han, J. Fang, Y. Zhang, H. Segawa, M. Grätzel, L. Han, *Nat. Energy* **2022**, DOI 10.1038/s41560-022-01038-1.

[4] S. Zhang, H. Wang, X. Duan, L. Rao, C. Gong, B. Fan, Z. Xing, X. Meng, B. Xie, X. Hu, *Adv. Funct. Mater.* **2021**, *31*, 2106495.

[5] S.-H. Turren-Cruz, A. Hagfeldt, M. Saliba, *Science* **2018**, *362*, 449.

[6] S. Gharibzadeh, P. Fassl, I. M. Hossain, P. Rohrbeck, M. Frericks, M. Schmidt, T. Duong, M. R. Khan, T. Abzieher, B. A. Nejand, F. Schackmar, O. Almora, T. Feeney, R. Singh, D. Fuchs, U. Lemmer, J. P. Hofmann, S. A. L. Weber, U. W. Paetzold, *Energy Environ. Sci.* **2021**, *14*,

5875.

[7] D. P. McMeekin, G. Sadoughi, W. Rehman, G. E. Eperon, M. Saliba, M. T. Horantner, A. Haghighirad, N. Sakai, L. Korte, B. Rech, M. B. Johnston, L. M. Herz, H. J. Snaith, *Science* **2016**, *351*, 151.

[8] D. B. Khadka, Y. Shirai, M. Yanagida, T. Noda, K. Miyano, *ACS Appl. Mater. Interfaces* **2018**, *10*, 22074.